UWB Fastly–Tunable 0.5–50 GHz RF Transmitter Based on Integrated Photonics

Fabio Falconi, Claudio Porzi, Antonio Malacarne, Filippo Scotti, Paolo Ghelfi, and Antonella Bogoni, *Member, IEEE*

(Top-Scored Paper)

***Abstract*—Currently, due to the 6G revolution, applications ranging from communication to sensing are experiencing an increasing and urgent need of software-defined ultra-wideband (UWB) and tunable radio frequency (RF) apparatuses with low size, weight, and power consumption (SWaP). Unfortunately, the coexistence of ultra-wideband and software-defined operation, tunability and low SWaP represents a big issue in the current RF technologies. Recently, photonic techniques have been demonstrated to support achieving the desired features when applied in RF UWB transmitters, introducing extremely wide operation and instantaneous bandwidth, tunable filtering, tunable photonics-based microwave mixing with very high port-to-port isolation, and intrinsic immunity to electromagnetic interferences. Moreover, the recent advances in photonics integration also allow to obtain very compact devices. In this article, to the best of our knowledge, the first example of a complete tunable software-defined RF transmitter with low footprint (i.e., on photonic chip) is presented exceeding the state-of-the-art for the extremely large tunability range of 0.5–50 GHz without any parallelization of narrower-band components and with fast tuning ($<$200 μs). This first implementation represents a breakthrough in microwave photonics.**

***Index Terms*—Microwave photonics, photonics integration ultra-wideband RF devices.**

I. Introduction

In THE last decade, the interest in software-defined ultra-wideband (UWB) and tunable radio frequency (RF) apparatuses with low size, weight, and power consumption (SWaP), has grown dramatically, pushed by the new 6G vision where new human-centric services will be made possible by combinations of connected smart devices, mobile robots, and avatars [1]. In this vision, RF equipment shall enable a large number of fundamental applications as UWB communications [2], robot localization mapping and control [3]–[6] and high precision radars [7]–[9], all of them contributing in revolutionizing our life style through breakthroughs in communications (e.g., intuitive ubiquitous connectivity), in medicine (e.g., wearable devices and tele-medicine), in security (e.g., pervasive situational awareness), in work processes (e.g., Industry 4.0), etc. Tunable UWB apparatuses, i.e., systems with a very large fractional bandwidth and an absolute bandwidth $>$500 GHz, also providing a wide frequency tunability, exhibit a low and tunable power spectral density that allow them being used as overlay signals in the same frequency range as existing legacy services without causing undue interferences [10], therefore bypassing the increasing issues of the overcrowded RF spectrum and the scarceness of available band.

In wireless communications, various UWB transmitters operating in the unlicensed band between 3.1 GHz and 10.6 GHz have been presented due to their benefits in term of high data rate, robustness to propagation fading, interference rejection, and coexistence with narrow band systems [11], [12]. UWB and frequency-agile communications offer additional advantages such as the implementation of the cognitive radio paradigm allowing to transmit in the less-crowded frequency regions [13], the undercover operations and the resistance to jamming thanks to the low spectral density and a superior obstacle penetration when working with long wavelengths [2], [14]. Moreover, fast frequency agility reduces the network latency and contributes to new functionalities as the tracking of high-speed moving users.

In the so-called Industry 4.0, precise location-aware applications also exploit low spectral density UWB signals for RF identification (RFID) [15]. Moreover, applications involving the use of robots have extended broadly, including services requiring the simultaneous operation of multiple robots, for which the precise localization & mapping and remote control can take advantage of rapidly tunable wideband RF connections [3]–[6] with bandwidth requirements in line with the 6G trends.

Moreover, such systems of robots are extending their applications from their traditional industry field to several other fields as military and medicine.

In advanced radars systems (as those foreseen in autonomous-driving vehicles), the broadband and fast frequency flexibility allows the implementation of a high-resolution and robust imaging, (including the case of moving targets) also integrating sensing and communication functionalities [16]. Moreover, UWB radar systems can detect the time-frequency signature of

Manuscript received August 14, 2021; revised October 25, 2021; accepted November 17, 2021. Date of publication December 16, 2021; date of current version March 16, 2022. This work was supported by the Italian Defense through the project DISTURB. *(Corresponding author: Antonella Bogoni.)*

Fabio Falconi, Claudio Porzi, and Antonella Bogoni are with the Sant'Anna School of Advanced Studies, 56124 Pisa, Italy (e-mail: fabio.falconi@santannapisa.it; claudio.porzi@santannapisa.it; antonella.bogoni@santannapisa.it).

Antonio Malacarne, Filippo Scotti, and Paolo Ghelfi are with the National Inter-University Consortium for Telecommunications (CNIT), 56124 Pisa, Italy (e-mail: antonio.malacarne@cnit.it; filippo.scotti@cnit.it; paolo.ghelfi@cnit.it).

Color versions of one or more figures in this article are available at https://doi.org/10.1109/JLT.2021.3135861.

Digital Object Identifier 10.1109/JLT.2021.3135861

the targets by digitally generating a wide variety of waveforms in different frequency ranges, tailored to the target type of interest [17].

High dynamic range and wideband operation across the full 0–40 GHz range and beyond are also required in electronic warfare systems, where such a kind of transmitters can be used as jammers for UWB communication links and radars [18]. Currently, the jammers work in specific RF bands, especially in the range 1–6 GHz, 5–18 GHz.

For all the applications mentioned above, an UWB transmitter is requested that must be able to provide fast frequency agility, and software-defined operation with the additional request of optimized SWaP for reducing the carbon footprint and fitting mobile platforms.

Unfortunately, the coexistence of ultra-wideband operation, reconfigurability (i.e., software-defined approach), tunability and low SWaP represents a big issue in the current RF technologies. In fact, large frequency tunability collide with the need to reduce SWaP, due to intrinsic limitations in state-of-the-art electronic and microwave components (in particular, tunable RF filters, mixers and oscillators). Currently the coverage of the UWB spectral range of interest is obtained through several narrower-band systems in parallel, thus leading to high SWaP and strongly limiting the applicability of the tunable UWB software-defined paradigm. In particular, a RF tunable UWB transmitter can be obtained with conventional technologies, exploiting a voltage-controlled oscillator (VCO) [19] combined with a wideband in-phase and quadrature (IQ) mixer or a battery of narrow band IQ mixers [20], [21], controlled by electrical switches and driven by a digital direct synthesizer (DDS). This solution is mainly limited in terms of tunability time (>1 ms) and range (<40 GHz) [19]. Moreover, the IQ mixers suffer from low image rejection, (<25 dBm).

On the other hand, photonic techniques are increasingly being proposed for implementing RF systems targeting those desired features [22], [23].

In the last few years, in fact, photonics has been demonstrating attractive features for microwave applications as extremely wide operating frequency range and instantaneous bandwidth [23]–[25], fast tunable filtering [26], tunable photonics-based microwave mixing with very high port-to-port isolation, and intrinsic immunity to electromagnetic interferences [27]. In [28], an UWB photonics-based transmitter for radio-over-fiber systems has been proposed, presenting an operating bandwidth larger than 60 GHz, although using, to operate at different frequencies, a bulky electronic synthesizer impeding desired low SWaP solutions. In [29], a filter-free photonics-based transmitter is presented operating up to 26 GHz, exploiting commercial off-the-shelf components.

Moreover, integrated photonics technologies are rapidly maturing, promising a breakthrough in RF systems through miniaturized, reconfigurable and wideband microwave photonics systems [30]–[32]. So far, most of the efforts have been focused on the optimization of the photonic integrated components for satisfying the RF system requirements, mainly based on the most mature platform of silicon photonics [24], [30], [33], [34].

In this paper, a prototype of an innovative widely tunable RF transmitter with unprecedented performance and enabled by integrated photonics is detailed [35], implemented on chip with

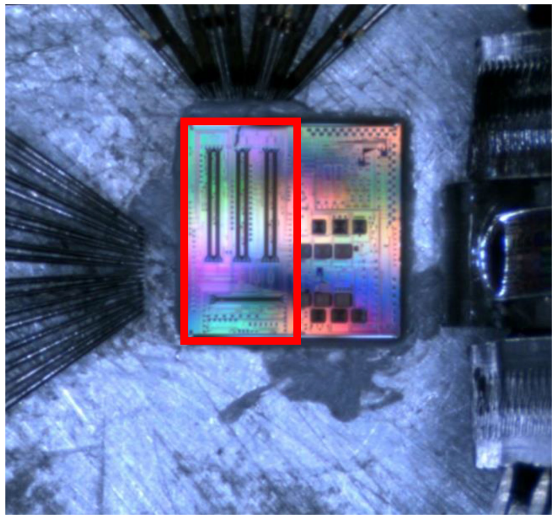

Fig. 1. The implemented silicon photonics chip onto a setup for characterization. The 0.5–50 GHz tunable RF transmitter is contained in the region outlined in red.

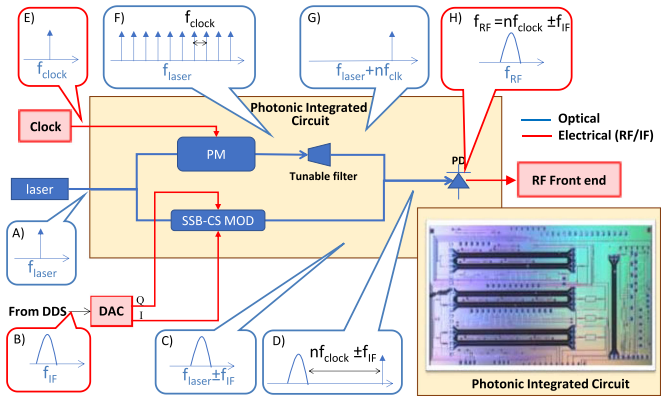

Fig. 2. Architecture of the photonics-based RF transmitter and picture of the PIC. DAC: digital-to-analog converter; PM: phase modulator; SSB-CS MOD: single sideband-carrier suppression modulator; PD: photodiode; (right): Detail of the PIC under test showing the RF (top) and DC (left) probes and the optical fiber array.

a CMOS-compatible Silicon-on-Insulator (SOI) technology as shown in Fig. 1, and demonstrating a working frequency range from 0.5 GHz to 50 GHz with fast tuning time <200 μs. This first implementation, although being a proof-of-concept with few limited performance, represents a breakthrough in microwave photonics, since it pioneers the concept of a complete UWB and tunable RF system on a photonic chip with the potential to significantly fully exceed the current state-of-the-art. At the same time, it also allows to experience the benefits and limitations of the silicon photonics platform for implementing complete microwave systems.

II. RF Transmitter Architecture and Single Component Characterization

Fig. 2 shows the architecture of the tunable photonics-based RF transmitter.

The generation of the tunable desired RF signal is based on the beating in a photodiode (PD) between an optical replica of the waveform to be transmitted, and a tunable optical carrier,

producing at the output an RF signal holding the waveform to be transmitted, translated at a center frequency equal to the detuning between the two optical signals. In more detail, the waveform to be transmitted is digitally generated through a direct digital synthesizer (DDS) and converted in the analog domain at intermediate frequency (IF) f_{IF} by means of a digital-to-analog converter (DAC) (inset B). The optical replica of the waveform is obtained through the modulation of an input laser (inset A) in single-sideband carrier-suppression (SSB-CS) format, as shown in the lower arm of the scheme in Fig. 2. This modulation is obtained by means of a dual-parallel pn junction-based Mach-Zehnder modulator (MZM) driven by the I and Q components of the waveform. This way, the obtained optical single-sideband signal (inset C) represents the optical replica of the original waveform.

On the other hand, a tunable optical carrier is obtained in the upper arm of the scheme of Fig. 2 by the tunable selection of one the optical lines out of an optical comb. The optical comb is generated by modulating the input laser by means of a pn junction-based phase modulator (PM) driven by an electrical fixed clock at frequency f_{clock} (inset E). This way, the comb line spacing is equal to f_{clock} (inset F). Then, a tunable optical bandpass filter selects one of the comb lines (inset G) at the desired frequency distance from the sideband (inset C). In particular, the selected line frequency is $f_{laser} \pm N f_{clock}$, where *N* is an integer number that can be chosen from 0 to the maximum usable line number within the comb, and its sign indicates the lines on the left or right of the input laser.

The SSB-CS modulator and the tunable optical filter are the most critical components of the scheme which required a custom design. The former one is responsible for providing a single sideband (the replica of the waveform in the optical domain) with excellent suppression of both the carrier and the second sideband, while the latter one shall select one line out of the full optical spectral comb with an excellent rejection.

The selected comb line and the single sideband are finally coupled (inset D) and injected into a Germanium-doped photodiode where they beat and generate an electrical replica of the waveform at the desired RF (inset H). This signal is then sent to an RF front-end before the transmission.

The proposed transmitter architecture allows for a continuous tunability: a coarse discrete tunability is achieved by the selection of the comb line, with a granularity corresponding to the clock frequency (line spacing), while the fine tunability for assuring a continuous tunability is achieved by the possibility to change the IF value up to the f_{clock}.

The photonic scheme (excluding the laser) has been implemented as a single photonic integrated circuit (PIC) exploiting the silicon-on-insulator (SOI) photonic platform at IMEC. Library blocks have been largely used (PM, PD, couplers/splitters), while the tunable filter and the architecture of the SSB-CS modulator (SSB-CS MOD) have been suitably designed. The obtained chip dimension is 5×2.5 mm^2. In the picture of the fabricated PIC in the insert of Fig. 2 it is possible to recognize the three long MZM structures, one used for implementing the PM and two for implementing the SSB-CS MOD.

TABLE I
SPECIFICATIONS OF THE SINGLE INTEGRATED PHOTONICS BLOCKS OF THE PHOTONICS-BASED TUNABLE RF TRANSMITTER

Integrated component	Design specifications	Measured specifications
Grating coupler		
Loss	3.0dB	3.3dB
SSB-CS MOD		
Bandwidth	> 5GHz	4GHz
Min loss	< 7dB	< 8dB
V_π	< 9V	8V
Suppression ratio	> 25dB	≥30dB (40dB for narrowband)
PM		
Bandwidth	> 5GHz	> 15GHz
Loss	4dB	4.1dB
V_π	< 9V	8V
Tunable Filter		
3-dB bandwidth	< 5GHz	< 4GHz
35dB bandwidth	< 10GHz	< 10GHz
Stop-band	> 5THz	> 6THz
Tunability range	> 10 nm	> 10 nm
Tuning time	<200 μs	<200 μs
In-band loss	≤ 10dB	10 dB
Photodiode		
Bandwidth	≥40 GHz	>45 GHz (with bias=4V)

As first step, the single components of the implemented chip are characterized, thanks to monitoring points specifically inserted in the photonic circuit. Then, the test of the PIC as a whole system is performed. For these tests, the PIC is placed on a thermo-electric cooler (TEC) that maintains its temperature with an accuracy of 0.01 °C. The signal from the input laser and the monitoring output signals are injected and extracted from the PIC by means of an array of fibers, while the electrical IF/RF signals and control signals are injected/extracted to/from the chip through a multiprobe, as shown in Fig. 1.

The RF clock frequency has been set to 5 GHz as best tradeoff between the expedience of using low f_{clock} values, i.e., dense optical comb, for reducing the maximum required IF for continuous tunability, consequently exploiting high-performance narrow-band DAC, and the expedience of relaxing the optical filter requirement in terms of bandwidth, i.e., coarse optical comb line spacing. In fact, both wideband DDS and DAC (>5 GHz) and narrow-band optical filters (<5 GHz) are critical components from a technological point of view, whereas 5 GHz DDS and DAC are available on the market with performance suitable for UWB RF transmitters and optical filters with 3 dB bandwidth of 5 GHz have been demonstrated [26].

Table I reports the main measured parameters compared to the design specifications, for each single component, obtained during the chip characterization with a $f_{clock} = 5$ GHz. It is worth to note that the characterization does not highlight significant worsening, rather, even better few specifications have been exceeded. As an example, the targeted photodiode bandwidth was >40 GHz, but the measured value is >45 GHz and generation of carriers up to 50 GHz have been obtained.

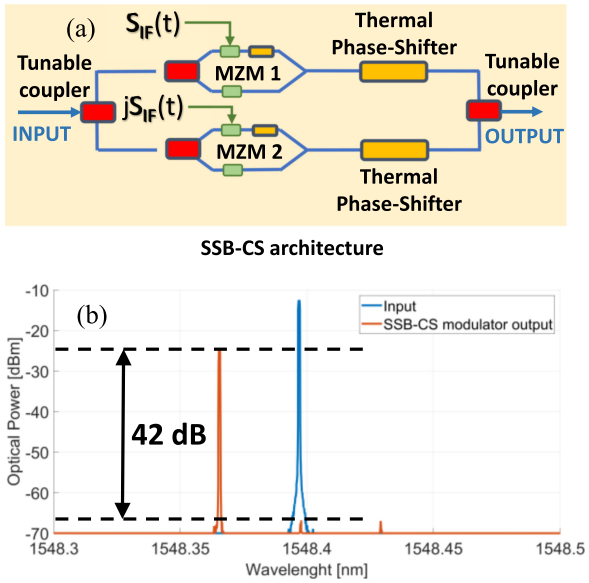

Fig. 3. (a) SSB-MOD architecture. (b) Measured optical spectrum at the input (blue curve) and at the output (red curve) of the SSB-CS MOD.

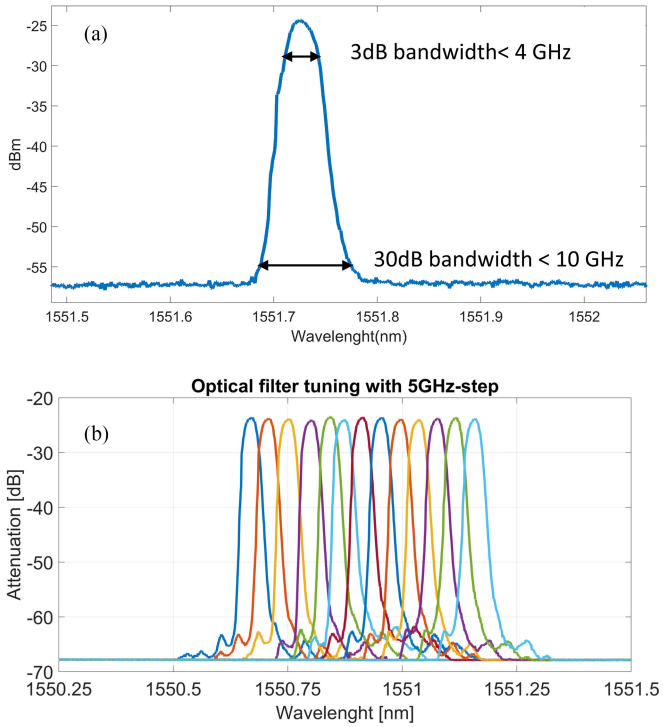

Fig. 4. (a) Tunable optical filter transmission. (b) Transmission of the optical filter for different positions of its central frequency, covering a range >50 GHz.

In particular, details of the characterization of the two custom components (SSB-CS modulator and tunable optical filter) are reported.

A. *Single-Sideband Carrier-Suppression Modulator*

With reference to Fig. 3(a), the SSB-CS modulator is composed of two MZMs in parallel which operates in a carrier suppression configuration by means of an appropriate control of the thermal phase shifters on each MZM structure and of the tunable couplers which appropriately balance the phases and the amplitudes respectively to suppress the carrier. Furthermore, it is possible to obtain the single sideband configuration by driving the two MZMs with two signals out of phase by 90° and balancing the phase and amplitude of the output signals of the Mach-Zehnder modulators through further thermal phase shifters and tunable coupler. As a result, at the output of the SSB-CS modulator a lateral band spaced from the wavelength of the original carrier by an amount equal to the frequency of the modulation signal (IF), is obtained. The main quality parameter of an SSB-CS modulator is the suppression of the carrier and the unwanted sideband compared to the main sideband. From Fig. 3(b) showing the measured optical spectra at the input (blue) and output (red) of the SSB-CS modulator, a suppression >40 dB is obtained. This result is comparable to the values obtained with a discrete lithium niobate optical modulator and exceeds the performance of the IQ mixers that generate the single sideband in conventional RF architectures with a suppression limited to 25 dB [20], [21]. However, once the SSB-CS bias condition is optimized in terms of carrier and unwanted sideband suppression for a given IF value, such a suppression depends on the IF value. It has been experimentally observed that the maximum IF deviation guaranteeing a suppression of the optical spurious modes ≥30 dB, once the modulator bias condition is optimized for a given IF, is 4 GHz (25 dB for a 5 GHz deviation). This aspect eventually limits the maximum signal bandwidth accordingly.

B. *Tunable Optical Filter*

The tunable optical filter has been realized as a cascade of phase-shifted Bragg gratings in a silicon waveguide [26]. In particular, it consists of a 4th-order filter, in which five Bragg gratings are separated by four grating "defects" a quarter wavelength-long, where the phase is carefully controlled by means of micro-heaters above the defects themselves. Its 3 dB bandwidth is as narrow as <4 GHz, while the 30 dB bandwidth is <10 GHz (see Fig. 4(a)) that is aligned with the state-of-the-art of optical filters. Consequently, the filter is able to select the desired line of the optical comb for f_{clock} (i.e., the comb frequency) ≥5 GHz with an extinction ratio >30 dB.

The tunability range of the filter is also verified, showing almost constant performance across 10 nm (i.e., 1.25 THz) within the optical C band (1530–1565 nm), In particular, Fig. 4(b) shows the transmission of the optical filter for different positions of its central frequency covering a range >50 GHz, confirming that the optical filter is suitable for generating RF signals with carrier frequency ≥50 GHz.

The filter tunability speed determines the RF transmitter tunability speed. This parameter is measured by varying the control signal of one of the 4 micro-heaters (one for each filter stage) with a step function, so as to be able to move the filter from a condition of misalignment with the test signal, to a condition of perfect alignment (see Fig. 5). By observing the time variation of the optical power at the filter output, a precise measure of the tunability speed can be obtained. The 10%-90%

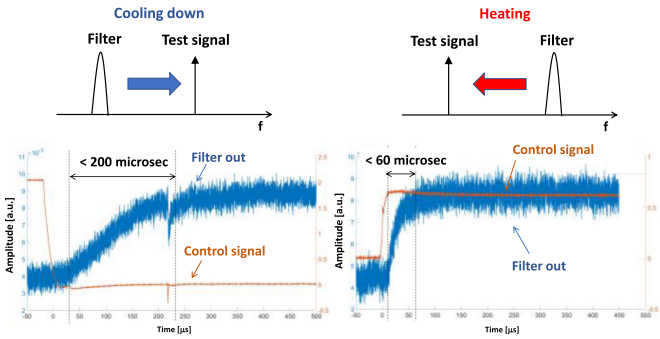

Fig. 5. Time behavior of the signal at the output of the filter as it passes from a condition of misalignment with the signal to one of alignment, in the case of movement towards higher frequencies for cooling (left) and movement towards lower frequencies for heating (right).

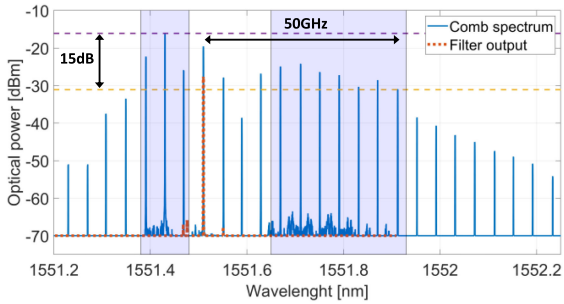

Fig. 6. Optical comb spectrum at the PM output and filter output selecting the laser carrier.

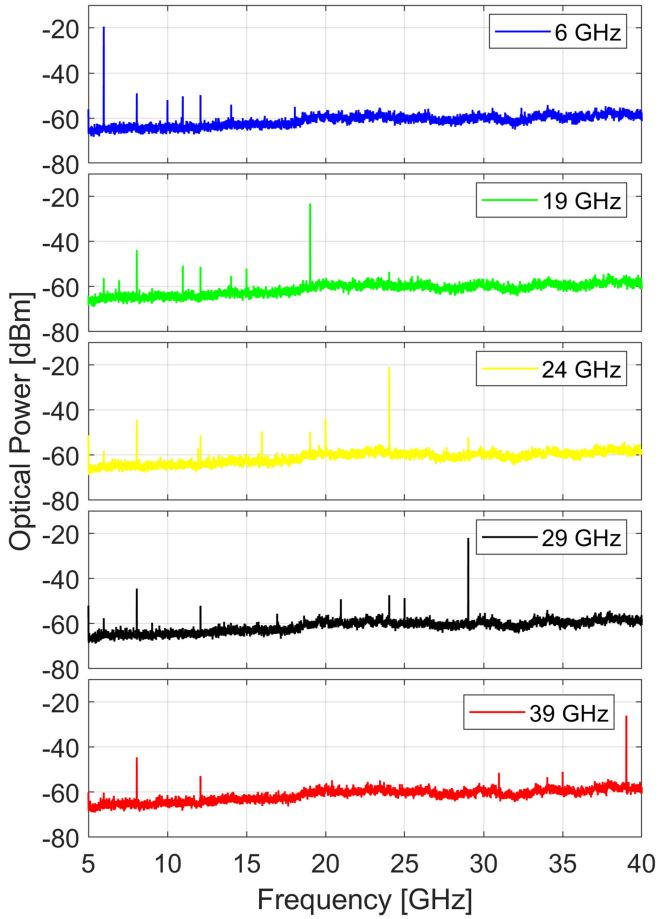

Fig. 7. RF carriers generated in C, X, Ku and Ka bands.

transient is less than 200 μs when the filter cools for shifting to higher frequencies (the sudden peak of the control signal around 220 μs is originated by the source meter employed for driving the heater), while it is faster (below 60 μs) when the filter is heated to shift it in the opposite spectral direction. This is because heating is applied by means of micro-resistors located exactly on top of the phase-shift defects in the Bragg gratings, so that an increase of the dissipated power in the micro-resistor affects the waveguide very quickly. Instead, cooling down the waveguide requires the excess heat accumulated within the PIC all around the heater to be dissipated in the chip, and hence to the TEC.

In both cases, the obtained filter tunability speed allows exceeding the transmitter tunability speed of conventional solutions limited to tunability time $>$1ms.

After characterizing the single integrated components, the PIC is tested as a tunable UWB transmitter system, checking the tunability and the signal purity in terms of phase noise and spurious-free dynamic range (SFDR). Finally, a communication experiment has been carried out in different RF bands.

III. System-Level Experimental Results

The architecture of the whole circuit can be deduced from Fig. 2, with the following additional details. An external laser is injected at the PIC input through a grating coupler (GC). The circuit includes a 3 dB 2$\times$2 multimode interference (MMI) splitter at the PM output for monitoring the generated optical spectral comb, and another MMI for monitoring the optical filter output. In addition, the 2$\times$2 MMI coupler responsible for recombination of the two arms, offers the possibility to reach either the internal PD or an output GC.

Fig. 6 shows the comb spectrum generated at the PM output and the corresponding filter output when tuned to select the laser carrier. The comb lines potentially used for RF generation up to 50 GHz are within the violet shaded regions. The power variation among those lines is 15 dB. This result has been achieved with a clock power of 27 dBm, corresponding to a peak-to-peak voltage of 14 V, and a reverse bias voltage of 4 V. This driving condition leads to a modulation regime involving both the reverse and direct polarity of the pn junction. Thus, in such a comb generation, both carrier-depletion and carrier-injection effects play a role, which is effective for generating a large number of comb lines up to clock frequencies of about 7 GHz, where carrier-injection dynamics exhibit a cut-off. The spectral asymmetry of the generated comb is an indication of the residual amplitude modulation associated with the plasma dispersion effect which is at the basis of fast phase modulation in silicon waveguides. Fig. 7 shows the results of the tunable generation of RF carriers across the C, X, Ku, K, and Ka bands, in case of sinusoidal waveform at $f_{IF} = 4$ GHz (used as upper or lower SSB). The bandwidth of the electrical spectrum analyzer limited the visualization of the generated RF signals to 40 GHz,

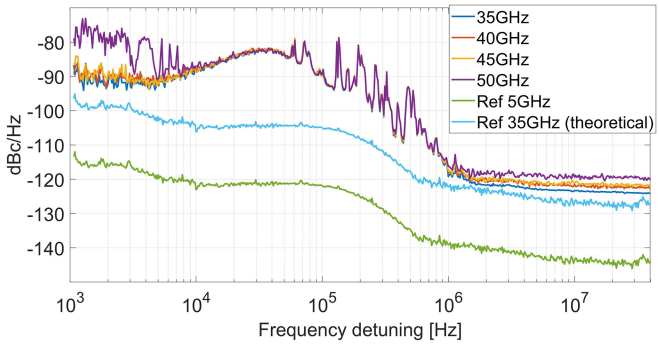

Fig. 8. Phase noise curves of the RF signal generated for different values of the carrier.

but RF signals have been generated up to 50 GHz (V band) as reported in the following. In all cases, the spurious tones are suppressed by more than 25 dB, see Fig. 7. Those tones are beating terms among useful signals, residual suppressed comb modes at the optical filter output, residual of the carrier and the unwanted sideband at the SSB-CS modulator output and, in some case, second-order sidebands. It is also worth to notice that the optical filter and the SSB-CS modulator, measured as stand-alone devices, guarantee an extinction ratio $>$30 dB and $>$40 dB, respectively. However, when tested as a system, the DC controls of the two devices turn out to induce mutual thermal crosstalk, leading to an increase of temperature fluctuations which affects the optimization of their working point and results in a reduction of the spurious rejection. In particular, carrier and unwanted sideband suppression at the SSB-CS modulator output decreases down to $>$30 dB. Thermal crosstalk reduction is possible by digging trenches between the components, acting as thermal insulators. In addition, temperature stability could be increased by improving thermal dissipation of the setup.

In order to study the quality of the generated tunable signals, the RF transmitter is characterized in terms of phase noise (PN). In this case only the 5 GHz RF clock is applied to the PIC, whereas the SSB-CS modulator is biased in such a way to minimize the loss on the optical carrier. Fig. 8 shows the PN power spectral density (PSD) of the RF carrier generated at high frequencies (35, 40, 45, 50 GHz), where a higher noise level is expected (the noise power increase is theoretically proportional to the frequency multiplication factor squared). The comparison with the reference clock signal at 5 GHz (in our case, a synthesizer) theoretically reported at the minimum analyzed frequency, i.e., 35 GHz (i.e., translated 17 dB upwards), is also shown in order to facilitate the comparison. PN curves are measured in a range 1 KHz–40 MHz of frequency offset from the nominal carrier frequency. The range has been chosen according to the requirements of communication applications and considering the limit of the instrument at 40 MHz. The PN of the signal generated at 45 and 50 GHz is also reported, even though this frequency is outside the accepted range of the employed electrical spectrum analyzer (Fig. 7).

The comparison of the phase noise curves presents at the extremes of the offset frequency, a gap in dBc/Hz in line with the expected ideal gap due to the different tested carrier frequency (i.e., 20 dB ideal gap from 5 GHz to 50 GHz).

Analyzing the excess noise in dBc/Hz approximately in the range 10 KHz–1 MHz, only part of it is due to the higher analyzed frequency. The shape of each obtained PN curves is clearly different from the reference PN. In particular, a pronounced wide "bell-shaped" peak centered at about 40 kHz is clearly visible and constant for each PN curve. As experimental investigations revealed, such additional phase noise term is originated by the current source (2602B by Keithley) used for driving each of the four thermal phase shifters employed for filter tuning, which exhibits a signal-to-noise ratio of only 12 dB (30 $\mathrm{mV_{RMS}}$ over a 500 mV DC term) for frequencies above 10 Hz. Such driving signal fluctuation causes temperature fluctuation at the heaters, which translates into a small frequency fluctuation of the filter spectral response. As spectral amplitude and phase of the filter response are drifting in frequency domain with dynamics in the frequency range where the "bell-shaped" PN disturb appears, this translates into an optical phase fluctuation on the optical comb line selected by the filter, eventually leading to the additional PN term on the generated RF tone after beating between filtered and laser lines, at the PD. By placing a lowpass filter at each current source output, such a noise term can be far mitigated, but at the expense of the filter tunability speed. An alternative solution is to employ lower-noise current sources.

Based on the reported phase noise curves, the temporal jitter of each generated RF tone is then calculated in the range 1–40 MHz, obtaining in all cases values lower than 170 fs, with a slight improvement for higher frequencies (from 169 fs at 35 GHz, down to 123 fs at 50 GHz) due to the constant contribution of temperature fluctuation, as stated before. The obtained jitter, although already comparable with the state-of-the-art of VCO (40 fs up to 32 GHz [19]), can be improved as previously discussed.

The software-defined photonics-based transmitter is also characterized in terms of its ability to generate a real communication signal, as shown in Fig. 9. The maximum signal bandwidth is limited by the DAC bandwidth, in this case 5 GHz, as well as the robustness of the carrier and unwanted sideband suppression condition versus the IF value. Indeed, a suppression $\geq$30 dB is guaranteed with a signal bandwidth $\leq$4 GHz (suppression $\approx$ 25 dB for signal bandwidth of 5 GHz). Here, the data signal is a standard 802.11g WiFi signal made by a 52 orthogonal frequency-division multiplexed (OFDM) 64-QAM subchannels, with a total information rate of 54 Mb/s and 20 MHz-analog bandwidth. The signal is generated at an intermediate frequency of 4.063 GHz. The clock signal is set again at 5 GHz. The up-converted version of the signal (at the carrier frequencies of 9, 14, 19, and 24 GHz), generated by the beating in the photodiode, is then analyzed using a vector signal analyzer. The performance is evaluated by measuring the error vector magnitude (EVM). Here the carrier frequency of the signal is limited by the bandwidth of the vector signal analyzer, which is $<$26 GHz. The EVM measurement detects variations $<$3 dB as the frequency varies, and a penalty with respect to the reference signal (i.e., obtained without tunable up-conversion) of less than 4 dB in all cases.

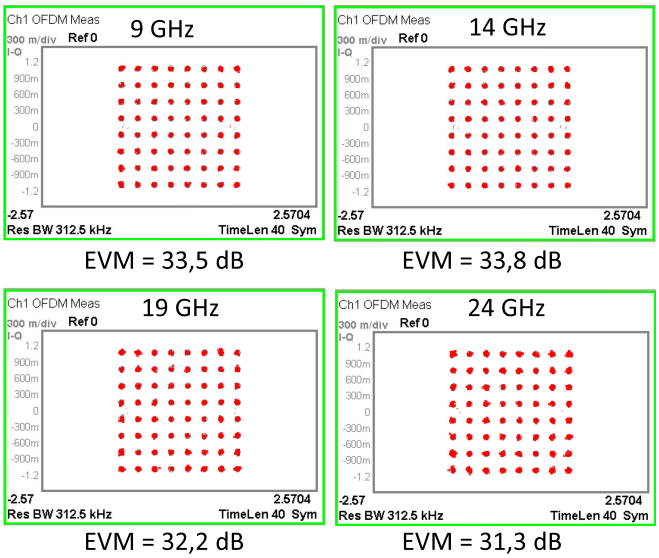

Fig. 9. 64QAM constellations generated at 9, 14, 19, 24 GHz (instrument limited to 26 GHz).

TABLE II
SPECIFICATIONS OF THE PHOTONICS-BASED TUNABLE RF TRANSMITTER

Photonics-based tunable RF transmitter	RF State of the art (VCO + IQ mixer)	Target specifications	Measured specifications	Potential performance
Tunability range	≤ 37 GHz	0.5GHz - 40GHz	0.5GHz - 50GHz	0.5GHz - 100GHz
Tunability speed	>1 ms	≤ 200µs	≤ 200µs	≤ 200µs
SFDR	≥25 dB	≥30 dB	≥25 dB	≥40 dB
Max instantaneous bandwidth	≥ 5GHz Limited by the DAC	≥ 5GHz Limited by the DAC	≤4GHz	5GHz
Jitter [1kHz-10MHz]	<40 fs	<50 fs	<200 fs	<30 fs
Input RF clock	-	5GHz	5GHz	5GHz
Conversion loss	< 10 dB	≤ 30dB	≈ 66 dB	< 10 dB
Waveform	Software-defined	Software-defined	Software-defined	Software-defined

IV. SYSTEM PERFORMANCE AND DISCUSSION

Table II (central column) summarizes all the obtained system performance and compares the obtained results with the RF state-of-the-art (left column) represented by the use of wideband VCO cascaded with a battery of narrower band IQ mixers. It is worth to note that the proposed photonics-based RF transmitter is a laboratory prototype, while the state-of-the-art comparison has been done with commercial components. In this sense the proposed technology has the potential to strongly improve its performance. For this reason, the achievable performance of the proposed solution after an optimization of the technological platform, as suggested by this proof-of-concept implementation, is also reported in the right column.

The implemented RF transmitter is able to generate tunable RF signals up to 50 GHz without any parallelization of narrower band components, and to provide fast frequency reconfigurability in less than 200 μs, enhancing the state-of-the-art tunability time (>1 ms). The SFDR in this specific implementation is limited to 25 dB, aligned with the RF state-of-the-art, due to thermal crosstalk between components as already discussed. However, after eliminating thermal crosstalk as explained in the following, RF transmitters with SFDR >40 dB can be obtained. In fact, the SSB-MOD is already providing a suppression ratio >40 dB, while optical filters with out-of-band rejection >40 dB at 5 GHz from the central frequency have already been demonstrated (rolloff ≥10 dB/GHz) [26], [34]. The maximum instantaneous bandwidth (B) is limited to 5 GHz, by the exploited DAC as in the RF state-of-the-art. The limit imposed by the photonic subsystem is much higher. It comes from the photodiode bandwidth (<45 GHz) that has to be $> f_{RF} + B/2$ in order to be able to generate the beating between the selected comb line and the optical sideband (i.e., the digitally generated waveform) with instantaneous bandwidth B at spectral distance f_{RF} from the laser. Integrated photodiodes have already been demonstrated to exceed a 100 GHz bandwidth [36], allowing for a RF signal generation beyond 100 GHz. The obtained jitter <170 fs is comparable with the state-of-the-art of electronic solutions limited to 40 GHz, but it is expected to be improved down to 30 fs with a more accurate temperature control of the optical filter as explained above. Moreover, the proposed solution guarantees software-defined waveforms as RF architectures.

The conversion loss of the implemented RF transmitter, defined as the ratio between the power of the IF input signal and the RF output signal, represents the main critical aspect of this implementation and also of all generic microwave photonics solutions: while RF technology provides values <10 dB, the state-of-the-art of microwave photonics systems based on silicon photonics presents a conversion loss ≤30 dB. In this implementation, the higher complexity of the architecture causes a measured conversion loss of 66 dB. However, this high value does not invalidate the demonstration of the potential of microwave photonics solutions for tunable UWB RF transceivers and it can be reduced as discussed in the following.

The relaxation of the footprint minimization (in this implementation is 5×2.5 mm^2) could contribute to reduce the conversion loss, helping in reducing few technological impairments as the thermal crosstalk that prevent the simultaneous optimization of all components. In particular, the behavior of the different components of the circuit depends on their temperature which is controlled by means of suitable electrical signals. As already mentioned, the tunability of the circuit is obtained through a thermal control. Unfortunately, considering the small size of the chip, a thermal crosstalk phenomenon occurs, i.e., when the temperature of a component is changed, the temperature of the adjacent components changes too, thus affecting their operating point. This phenomenon induces a deviation of the working points of the components from the optimal conditions, introducing a penalty on the generated signal, especially in terms of conversion loss and spurious rejection. This criticality was highlighted during the characterization phase, generating a penalty of >5 dB on the spurious rejection in the generated RF signals. A possible solution to this problem is to include digging trenches between the components, acting as thermal insulators and thus allowing a reduction of the thermal crosstalk.

The conversion loss can also be improved reducing the losses in the photonic circuit. Input/output GCs loss, measured to be 3.3 dB per GC, can be in principle decreased down to approximately 1 dB or below [37], [38]. In-band filter loss, measured to be up to 10 dB, can be decreased down to approximately 3 dB by using a long-cavity design with reduced BG mirrors

reflectivity, which allows to maintain a similar photon lifetime in the coupled-resonators (hence filter bandwidth) as in the current design while taking advantage of the lower propagation loss in the long uncorrugated waveguide section with respect to the portion of the cavity that extends within the distributed BG mirrors, as discussed for instance in [39]. Monitor MMI splitters at both PM output and optical filter output, can be removed in a final prototype version, or custom MMIs can be considered, where only few percentage of the power can be employed for monitoring purposes. Another possibility is to introduce optical amplification stages. Optical amplifiers cannot be realized in silicon photonics, but their implementation requires a hybrid integration, i.e., a technology capable of putting together PICs realized with different materials. Such approach would permit to integrate active components, i.e., optical amplifiers, on silicon platform. Recent achievements concerning semiconductor optical amplifiers (SOAs) bonded on SOI wafer, demonstrate a potential optical gain approaching 30 dB [40]. Another technological advance for reducing the conversion loss consists in reducing the $V\pi$, i.e., the voltage necessary for modulators to transfer intermediate frequency signals to the optical domain, and reduce their optical attenuation and nonlinearities. To date, the best technology for modulator implementation is the bulk lithium niobate (LN), a non-integrated technology that has dominated the telecom industry scene for decades, where the Pockels electro-optical effect warrants implementation of low attenuation and highly linear modulators. Recently, integrated lithium niobate on insulator (LNOI) technology has been developed, which enables on-chip LN modulators with very low $V\pi$ and with dimensions typical of photonic chips [41]–[43]. Another option to reduce $V\pi$ without involving different platforms, might be to increase the length of the pn-junction in the silicon phase modulators, optimizing the tradeoff between required modulation bandwidth and $V\pi$, during a final engineering process of the circuit. For instance, in the presented design, modulators included in the SSB-CS stage exhibit a modulation bandwidth far above the applied IF value. Longer pn-junctions would have reduced the conversion loss. All the above considerations allow to estimate a possible improved conversion loss $\leq$10 dB, aligned with the RF state-of-the-art, if an hybrid photonic integration approach is exploited for integrating active components with LNOI modulators.

V. Conclusion

A breakthrough implementation of a 0.5–50 GHz tunable RF transmitter based on integrated photonics has been presented. It has been obtained through a tunable up-conversion in the optical domain of a digitally generated waveform at intermediate frequency, completely avoiding the parallelization of components with limited bandwidth. The chip characterization confirms the potential of microwave photonics for overcoming the current challenges of RF systems in terms of fast frequency agility and broadband coverage, maintaining a low SwAP and meeting the RF transmitter future requirements in the field of communications and sensing for a large range of applications. Moreover, this first implementation brought out the main technological issues of silicon photonics that will drive further developments of hybrid integrated photonics platforms. In a dual way, the same microwave photonic solution can allow to implement in the optical domain a down-conversion of a received RF signal to intermediate frequency, resulting in an ultra-wideband tunable RF receiver [44]. In this sense the reported demonstration represents a fundamental step toward the implementation of a building block for next generation flexible and ultra-wideband transceivers to be exploited in several emerging markets.

References

[1] M. Maier and A. Ebrahimzadeh, "The 6G Vision," in *Toward 6G: A New Era of Convergence*, 1st ed., Wiley-IEEE Press, 2021, pp. 1–17, doi: 10.1002/9781119658054.ch1.

[2] W. Paper, "Cisco visual networking index: Global mobile data traffic forecast update 2017–2022," 2019. Accessed: Aug. 2021. [Online]. Available: https://s3.amazonaws.com/media.mediapost.com/uploads/CiscoForecast.pdf

[3] L. Han, B. Dzodzo, H. Qian, and Y. Xu, "Chapter 3.1," in *The State of the Art in Mapping and Navigation for Household Service*, Y. Xu, H. Qian, and X. Wu, Eds. Household Service Robotics, Orlando, FL, USA: Academic, 2015, pp. 117–128. [Online]. Available: https://doi.org/10.1016/B978-0-12-800881-2.00007-4

[4] S. Saeedi, M. Trentini, M. Seto, and H. Li, "Multiple-Robot simultaneous localization and mapping: A review," *J. Field Robot.*, vol. 33, no. 1, pp. 3–46, Jan. 2016. [Online]. Available: https://doi.org/10.1002/rob.21620

[5] X. Zhu, J. Yi, J. Cheng, and L. He, "Adapted error map based mobile robot UWB indoor positioning," *IEEE Trans. Instrum. Meas.*, vol. 69, no. 9, pp. 6336–6350, Sep. 2020. doi: 10.1109/TIM.2020.2967114.

[6] F. J. Perez-Grau, F. Caballero, L. Merino, and A. Viguria, "Multi-modal mapping and localization of unmanned aerial robots based on ultra-wideband and RGB-D sensing," in *Proc. IEEE/RSJ Int. Conf. Intell. Robots Syst.*, Vancouver, BC, Canada, 2017, pp. 3495–3502. doi: 10.1109/IROS.2017.8206191.

[7] J.-Y. Park *et al.*, "Preclinical evaluation of a noncontact simultaneous monitoring method for respiration and carotid pulsation using impulse-radio ultra-wideband radar," *Sci. Rep.*, vol. 9, no. 1, p. 11892, Aug. 2019, doi: 10.1038/s41598-019-48386-9

[8] D. B. Issa *et al.*, "Reconfigurable UWB transceiver for biomedical sensor application," *BioNanoSci.*, vol. 7, pp. 11–25, 2017. [Online]. Available: https://doi.org/10.1007/s12668-016-0384-9

[9] J. W. Choi, D. H. Yim, and S. H. Cho, "People counting based on an IR-UWB radar sensor," *IEEE Sensors J.*, vol. 17, no. 17, pp. 5717–5727, Sep. 2017, doi: 10.1109/JSEN.2017.2723766.

[10] A. F. Molisch, "Ultra-wideband communications: An overview," *URSI Radio Sci. Bull.*, vol. 2009, no. 329, pp. 31–42, Jun. 2009, doi: 10.23919/URSIRSB.2009.7909730.

[11] M. Z. Win, D. Dardari, A. F. Molisch, W. Wiesbeck, and J. Zhang, "History and applications of UWB," *Proc. IEEE*, vol. 97, no. 2, pp. 198–204, Feb. 2009, doi: 10.1109/JPROC.2008.2008762.

[12] G. Lee, J. Park, J. Jang, T. Jung, and T. W. Kim, "An IR-UWB CMOS transceiver for high-data-rate, low-power, and short-range communication," *IEEE J. Solid-State Circuits*, vol. 54, no. 8, pp. 2163–2174, Aug. 2019.

[13] W. S. H. M. W. Ahmad *et al.*, "5G Technology: Towards dynamic spectrum sharing using cognitive radio networks," *IEEE Access*, vol. 8, pp. 14460–14488, 2020, doi: 10.1109/ACCESS.2020.2966271.

[14] X. Liang *et al.*, "Ultra-Wideband impulse radar through-wall detection of vital signs," *Sci. Rep.*, vol. 8, no. 13367, 2018. [Online]. Available: https://doi.org/10.1038/s41598-018-31669-y

[15] Y. Zhou, C. L. Law, and J. Xia, "Ultra low-power UWB-RFID system for precise location-aware applications," in *Proc. IEEE Wireless Commun. Netw. Conf. Workshops*, Paris, France, Jun. 2012, pp. 154–158, doi: 10.1109/WCNCW.2012.6215480.

[16] D. Ma, N. Shlezinger, T. Huang, Y. Liu, and Y. C. Eldar, "Joint radar-communication strategies for autonomous vehicles: Combining two key automotive technologies," *IEEE Signal Process. Mag.*, vol. 37, no. 4, pp. 85–97, Jul. 2020.

[17] J. D. Taylor, *Advanced Ultrawideband Radar: Signals, Targets, and Applications*, Boca Raton, FL, USA: CRC Press, Dec. 2019.

[18] M. Frater and M. J. Ryan, *Electronic warfare for the digitized battlefield*, Norwood, MA, USA: Artech House, 2001.
[19] [Online]. Available: https://www.analog.com/en/products/adf4371.html
[20] [Online]. Available: https://www.av-iq.com/avcat/ctl1642/index.cfm?manufacturer=analog-devices&product=hmc8038
[21] [Online]. Available: https://www.qorvo.com/products/frequency-converters/mixers
[22] P. Ghelfi, F. Laghezza, and A. Bogoni, *Photonics for Radar Networks and Electronic Warfare Systems* (Radar, Antennas and Electromagnetics Series), IET Digital Library, Scitech Pub. Inc., May 2019.
[23] H. G. de Chatellus, L. R. Cortés, C. Schnébelin, M. Burla, and J. Azaña, "Reconfigurable photonic generation of broadband chirped waveforms using a single CW laser and low-frequency electronics," *Nature Commun.*, vol. 9, no. 2438, pp. 1–12, 2018.
[24] J. Tang, B. Zhu, W. Zhang, M. Li, S. Pan, and J. Yao, "Hybrid Fourier-domain mode-locked laser for ultra-wideband linearly chirped microwave waveform generation," *Nature Commun.*, vol. 11, no. 3814, pp. 1–8, 2020.
[25] E. Ruggeri *et al.*, "A 5G fiber wireless 4Gb/s WDM fronthaul for flexible 360 °Coverage in V-Band massive MIMO small cells," *J. Lightw. Technol.*, vol. 39, no. 4, pp. 1081–1088, Feb. 2021, doi: 10.1109/JLT.2020.3029608.
[26] C. Porzi, G. J. Sharp, M. Sorel, and A. Bogoni, "Silicon photonics high-order distributed feedback resonators filters," *IEEE J. Quantum Electron.*, vol. 56, no. 1, pp. 1–9, Feb. 2020, doi: 10.1109/JQE.2019.2960560.
[27] P. Ghelfi *et al.*, "A fully photonics-based coherent radar system," *Nature*, vol. 507, pp. 341–345, Mar. 2014.
[28] O. Omomukuyo, M. P. Thakur, and J. E. Mitchell, "Experimental performance analysis of MB-OFDM ultra-wideband radio-over-fiber signals in the 60-GHz band using a commercially-available DFB laser," in *Proc. 14th Int. Conf. Transp. Opt. Netw.*, 2012, doi: 10.1109/ICTON.2012.6254424.
[29] D. Onori, F. Scotti, F. Laghezza, A. Bogoni, and P. Ghelfi, "A software-defined and filter-free 0–26.5 GHz ultra-wideband RF transmitter enabled by photonics," in *Proc. Eur. Radar Conf.*, 2017, pp. 529–532, doi: 10.23919/EURAD.2017.8249264.
[30] D. Marpaung, J. Yao, and J. Capmany, "Integrated microwave photonics," *Nature Photon.*, vol. 13, pp. 80–90, 2019. [Online]. Available: https://doi.org/10.1038/s41566-018-0310-5
[31] F. Falconi *et al.*, "A combined radar & lidar system based on integrated photonics in silicon-on-insulator," *J. Lightw. Technol.*, vol. 39, no. 1, pp. 17–23, Jan. 2021, doi: 10.1109/JLT.2020.3023496.
[32] S. Li *et al.*, "Chip-based microwave-photonic radar for high-resolution imaging," *Laser & Photonics Reviews*, vol. 14, no. 10, p. 1900239, 2020, doi: 10.1002/lpor.201900239.
[33] R. Maram, S. Kaushal, J. Azaña, and L. R. Chen, "Recent trends and advances of silicon-based integrated microwave photonics," *Photonics*, vol. 6, no. 1–13, 2019. [Online]. Available: https://doi.org/10.3390/photonics6010013
[34] P. Dong *et al.*, "GHz-bandwidth optical filters based on high-order silicon ring resonators," *Opt. Express*, vol. 18, no. 23, pp. 23784–23789, 2010.
[35] F. Falconi *et al.*, "Photonics-based tunable 1–50 GHz RF transmitter on silicon chip," in *Proc. Opt. Fiber Commun. Conf. Exhib.*, 2021, Paper Tu5F.2.
[36] S. Lischke *et al.*, "Ge photodiode with -3 dB OE bandwidth of 110 GHz for PIC and ePIC platforms," in *Proc. IEEE Int. Electron. Devices Meeting*, Mar. 2020, pp. 7.3.1–7.3.4, doi: 10.1109/IEDM13553.2020.9372033.
[37] X. Chen, C. Li, C. K. Y. Fung, S. M. G. Lo, and H. K. Tsang, "Apodized waveguide grating couplers for efficient coupling to optical fibers," *IEEE Photon. Technol. Lett.*, vol. 22, no. 15, pp. 1156–1158, Aug. 2010.
[38] Y. Ding, C. Peucheret, H. Ou, and K. Yvind, "Fully etched apodized grating coupler on the soi platform with 0.58 dB coupling efficiency," *Opt. Lett.*, vol. 39, no. 18, pp. 5348–5350, 2014.
[39] C. Porzi, F. Falconi, M. Sorel, P. Ghelfi, and A. Bogoni, "Flexible millimeter-wave carrier generation up to the Sub-THz with silicon photonics filters," *J. Lightw. Technol.*, vol. 39, no. 24, pp. 7689–7697, Dec. 2021.
[40] D. Néel *et al.*, "Novel technology of III die-bonded SOI photonic integrated circuits," *Proc. SPIE*, vol. 11880, 2021, pp. 35–45.
[41] T. Ren *et al.*, "An integrated low-voltage broadband lithium niobate phase modulator," *IEEE Photon. Technol. Lett.*, vol. 31, no. 11, pp. 889–892, Jun. 2019, doi: 10.1109/LPT.2019.2911876.
[42] M. Xu *et al.*, "High-performance coherent optical modulators based on thin-film lithium niobate platform," *Nature Commun.*, vol. 11, 2020, Art. no. 3911.
[43] P. Kharel, C. Reimer, K. Luke, L. He, and M. Zhang, "Breaking voltage–bandwidth limits in integrated lithium niobate modulators using micro-structured electrodes," *Optica*, vol. 8, no. 3, pp. 357–363, 2021. [Online]. Available: https://doi.org/10.1364/OPTICA.416155
[44] D. Onori *et al.*, "A Photonically-enabled compact 0.5–8.5 GHz RF scanning receiver," *IEEE J. Lightw. Technol.*, vol. 36, no. 10, pp. 1831–1839, May 2018.